DOT/FAA/AR-00/50

Office of Aviation Research
Washington, D.C. 20591

A Methodology to Predict the Empennage In-Flight Loads of a General Aviation Aircraft Using Backpropagation Neural Networks

February 2001

Final Report

U.S. Department of Transportation
Federal Aviation Administration

NOTICE

This report is available at the Federal Aviation Administration William J. Hughes Technical Center's Full-Text Technical Reports page: actlibrary.tc.faa.gov in Adobe Acrobat portable document format (PDF).

Technical Report Documentation Page

1. Report No.	2. Government Accession No.	3. Recipient's Catalog No.
DOT/FAA/AR-00/50		

4. Title and Subtitle	5. Report Date
A METHODOLOGY TO PREDICT THE EMPENNAGE IN-FLIGHT LOADS OF A GENERAL AVIATION AIRCRAFT USING BACKPROPAGATION NEURAL NETWORKS	February 2001
	6. Performing Organization Code
7. Author(s)	8. Performing Organization Report No.
David Kim and Maciej Marciniak	
9. Performing Organization Name and Address	10. Work Unit No. (TRAIS)
Embry-Riddle Aeronautical University 600 S. Clyde Morris Blvd. Daytona Beach, FL 32114	11. Contract or Grant No. 93-G-026
12. Sponsoring Agency Name and Address	13. Type of Report and Period Covered
U.S. Department of Transportation Federal Aviation Administration Office of Aviation Research Washington, DC 20591	Final Report
	14. Sponsoring Agency Code ACE-100

15. Supplementary Notes

The FAA William J. Hughes Technical Center Program Manager was Thomas DeFiore.

16. Abstract

Backpropagation neural networks were used to predict strains resulting from maneuver loads in the empennage structure of a Cessna 172P. The purpose of this research was to develop a methodology for the prediction of strains in the tail section of a general aviation aircraft that would not require installation of strain gages and to determine the minimum set of sensors necessary for a prediction suitable for small aircraft. This report provides a methodology for determining in-flight tail loads using neural networks. The method does not require the installation of strain gages on each airplane. It is an inexpensive and effective technique for collecting empennage load spectra for small transport airplanes already in service where installation of strain gages are impractical. Linear accelerometer, angular accelerometer, rate gyro, and strain gage signals were collected in flight using DAQBook portable data acquisition system for dutch-roll, roll, sideslip left, sideslip right, stabilized g turn left, stabilized g turn right, and push-pull maneuvers at airspeeds of 65 KIAS, 80 KIAS, and 95 KIAS. The sensor signals were filtered and used to train the neural networks. Modular neural networks were used to predict the strains. The horizontal tail neural network was trained with c.g. Nz and x-, y-, and z-axis angular accelerometer signals and predicted 93% of all strains to within 50 με of measured values. The vertical tail neural network predicted 100% of all strains to within 50 με of measured values.
.

17. Key Words	18. Distribution Statement
Flight loads, Empennage, Flight recorder, General aviation	This document is available to the public through the National Technical Information Service (NTIS) Springfield, Virginia 22161.

19. Security Classif. (of this report)	20. Security Classif. (of this page)	21. No. of Pages	22. Price
Unclassified	Unclassified	44	

TABLE OF CONTENTS

LIST OF FIGURES

LIST OF TABLES

EXECUTIVE SUMMARY

This report provides a methodology for determining in-flight tail loads using neural networks. It does not require the installation of strain gages on each airplane. It is an inexpensive and effective technique for collecting empennage load spectra for small transport airplanes already in service where installations of strain gages are impractical.

1. INTRODUCTION.

1.1 OVERVIEW.

The Code of Federal Regulation (CFR) Part 23 requires that the wing, pressurized fuselage, and empennage of an aircraft must not fail within their expected lifetimes due to damage caused by the repeated loads typical to its operations. This requirement generates the need for evaluation of fatigue life of critical aircraft structures. Most commonly, the fatigue life is determined using the Palmgren-Miner Linear Cumulative Damage Theory. In order to calculate fatigue life of a given structure accurately using this method, one must know the loading on this structure throughout its lifetime. The most critical of these structures are the wing and the empennage.

There is some information on wing in-flight loads of general aviation aircraft that can be used to determine fatigue life of such structures. However, there is very little such information on empennage in-flight loads. Clearly, an efficient, practical, and cost-effective method of determining the empennage in-flight loads in general aviation aircraft is much needed.

Such a method could be used to create an empennage fatigue loads spectra. This spectra, together with the existing fatigue load data for wings, could be used to determine the appropriate flight loads spectra for a newly designed or built aircraft. Such a spectra could be used for designing empennage structures.

In addition to building the loads spectra, an in-flight load monitoring system could be used to keep track of accumulated service loads usage of an airframe. This would be of special interest to operators of general aviation aircraft since the severity of the usage of the aircraft that fall into this category could vary widely even for the same aircraft model. For example; aircraft used in training environments or pipeline inspections are likely to experience flight loads that approach the design limits more frequently than aircraft flown occasionally for recreational purposes. Despite this wide usage spectrum, all general aviation operators are required to conform to a maintenance schedule that was established hypothetically for the most severe aircraft operation.

One of the requirements for the successful implementation of this type of structural monitoring system for general aviation is it must be inexpensive. If a large comprehensive in-flight load usage spectra is to be created, a large number of aircraft used in a variety of flight conditions will have to be monitored. This suggests that the best system for the task would be one that is easy (and inexpensive) to install and maintain. It should also not intrude into normal operations of the aircraft. If it is to be widely adopted as a flight loads monitoring tool, the unit price must be low enough to attract the interest of small aircraft fleet operators and owners. For either application, it would be undesirable to install transducers of any kind on structural components for direct measurements. A system similar to the National Aeronautics and Space Administration (NASA) VGH (velocity, load factor, and altitude) recorder is ideal [1]. With the VGH system, the data recorded near the aircraft center of gravity (c.g.) is used to determine loads on extremities like the empennage. Initial work performed in this study indicated that while there appears to be some relationship between acceleration in the y direction (c.g. Ny) and the strain in the vertical tail, there is only a very weak relationship between the acceleration in the z direction (c.g. Nz) and the strain in the horizontal tail. Thus, the main focus of the present research is to develop another

method of relating data collected near the aircraft c.g. to strains occurring elsewhere, specifically in the empennage structure.

1.2 PREVIOUS RESEARCH.

The NASA VGH program was the largest and the longest running in-flight load monitoring program for general aviation aircraft. In the United States, it also represents the only comprehensive flight loads spectra monitoring program. This program started in the early 1960s and continued until 1982. In that time 42,155 hours of data were collected on 105 airplanes. Airplanes were chosen from nine usage groups: twin-engine executive, single-engine executive, personal, instructional, commercial survey, aerial applications (fire fighting, etc.), aerobatic, commercial, and float operations. Data for 35,286 hours of operation from 95 airplanes were evaluated and presented as a part of a fatigue evaluation method for wings in report AFS-120-73-2 [2]. The final report on the VGH project—DOT/FAA/CT-91/20—was published in 1993. As the original NASA VGH program focused on normal (z direction) accelerations, the need for a similar program to evaluate fatigue life of vertical aerodynamic surfaces such as fins, rudders, and winglets, was expressed by the authors of the final report. Since only the accelerations near the center of gravity were measured, the NASA project left the problem of fatigue loads on empennage structure largely unaddressed [1].

Other load-monitoring programs have been completed outside the United States. For example, a cooperative effort between the Dutch National Aerospace Laboratory (NLR), the Dutch National Airline (KLM), and the Fokker Company resulted in a year long in-flight tail load monitoring program [3]. In this program, strain was measured on the tail of a Fokker 100 airliner. Data were collected over a period of one year of commercial service. Large amounts of useful data were collected, but for a large fleet of aircraft, the method used—direct measurement using strain gages—is not considered to be a viable approach to the problem presented in the overview (section 1.1) due to the costs of installation and maintenance.

There has also been a limited amount of work done in the area of flight loads prediction. Research done by the U.S. Navy has successfully demonstrated that it is possible to predict strains at some point of the structure from the flight parameter data collected at another point. In this case, c.g. Nz, wing sweep angle, angle of attack, roll rate, Mach number, altitude, weight-on-wheels indicator, and an indicator for takeoff, landing, and peak-or-valley data were used to predict strain at a point on aft fuselage of an F-14B aircraft. The correlation coefficients were from 0.93 to 0.97 between the predicted and measured strain [4].

Another research effort by the U.S. Navy successfully employed neural networks to predict loads experienced in flight by the main rotor blades of a helicopter. Neural networks were chosen because of the difficulties associated with attempts to directly measure loads in a rotating system. The inputs to the network were load factor, longitudinal, lateral, pitch, roll, and yaw accelerations, airspeed, aircraft mass, rate of climb, rotor speed, rotor control servo position, and stabilator position. The correlation coefficients were from 0.93 to 0.96 between the predicted and the actual load [5].

Similar work was accomplished at Virginia Polytechnic Institute and State University using neural networks to predict the time-varying mean and oscillatory components of the tail boom bending load and the pitch link loads. For this application the input variables were pitch rate, roll rate, yaw rate, vertical acceleration, lateral acceleration, longitudinal acceleration, longitudinal control position, and lateral control position. The correlation coefficients were from 0.907 to 0.977 between the predicted and actual loads [6].

1.3 CURRENT APPROACH.

Despite the fact that multiple linear regression analysis resulted in a small correlation coefficient between accelerations measured in the vicinity of the aircraft c.g. and corresponding strains experienced by the empennage structure, it is not unreasonable to assume that there nevertheless should be some, presumably nonlinear, relationship between these quantities. The purpose of this study was to employ artificial neural networks to define such a relationship, if one exists.

Neural networks are capable of modeling nonlinear relationships between variables and offer a good chance of finding the solution. Two neural networks were used: one to predict the strains in the vertical tail and one to predict the strains in the horizontal tail. The work concentrated on finding the minimum instrumentation sensor set needed to accurately predict these strains, the minimum threshold value of significant strain, and the correlation between sensor output and the empennage flight loads of a Cessna 172. The inputs into the neural networks were provided by the signals collected in flight from the following instruments: three rate gyros and three angular accelerometers measuring the angular velocities and the angular accelerations about each of the aircraft axes, two linear accelerometers measuring the z-axis and the y-axis accelerations in the vicinity of the aircraft c.g., and two linear accelerometers measuring the z-axis and the y-axis accelerations in the tail cone. In addition, the aircraft had sensors for airspeed, pressure altitude, angle of attack, and sideslip measurements. The test bed for this research was a Cessna 172P. This aircraft was equipped with the linear accelerometers and strain gages on the aircraft primary structures. The rate gyros, angular accelerometers, and a portable data acquisition system were added.

Various combinations of the signals from these instruments were used as inputs into the neural networks. The networks generated during the research are only valid for the Cessna 172P model. To verify this approach and to develop neural networks for other aircraft models, the methodology needs to be applied in a similar fashion to those aircraft.

2. BACKGROUND THEORY.

2.1 NEURAL NETWORKS DESCRIPTION.

Artificial neural networks (or simply neural networks) are information processing systems that attempt to emulate some of the processing characteristics of the human brain [7]. Much like its biological counterpart, an artificial neural network consists of a large number of heavily interconnected simple processing elements. This brain-like organization gives the neural network parallel processing and learning capability.

The above characteristics make the neural networks useful for tasks that are either impossible or very difficult to accomplish using traditional computer programs. These tasks include

a. Pattern Classification: recognition and separation of patterns contained in data.
b. Prediction: determination of a value of a variable from a set of given values.
c. Conceptualization: determination of conceptual relationships within datasets.
d. Filtering: smoothing of a noisy signal.
e. Optimization: determination of the optimal values.

All of the above functions can be accomplished by simply altering the arrangement and number of processing elements.

Most neural networks, like the human brain, require iterative feedback training. Depending on the task at hand, either supervised or unsupervised training is needed. Supervised training means that the neural network is given a set of input-correct output pairs to train on. Unsupervised training means that the network is only given the input data to train on. In general, prediction requires supervised training, while classification, conceptualization, filtering, and optimization use unsupervised training.

Neural networks are sometimes viewed as "black boxes." There is no easy way of tracing or mathematically representing the internal processes occurring within a network. This is especially true for the more complex networks that may consist of hundreds of processing elements and thousands of connections. Also, finding the right arrangement of processing elements for a given problem usually involves significant amounts of trial and error, as there is no systematic method presently available for determining this information *a priori*.

2.2 COMPONENTS OF NEURAL NETWORKS.

Neural networks have two main components: the processing elements and the connections between them. The processing elements, sometimes called neurons, units, cells, or nodes, function as information processors, and the connections function as information storage. Figure 1 shows a diagram of a processing element with connections going in and out of it. Each processing element first calculates a weighted sum of the input signals, then applies a transfer function to this sum and outputs the result. Transfer functions are generally nonlinear. Nonlinear functions are required to solve nonlinear problems.

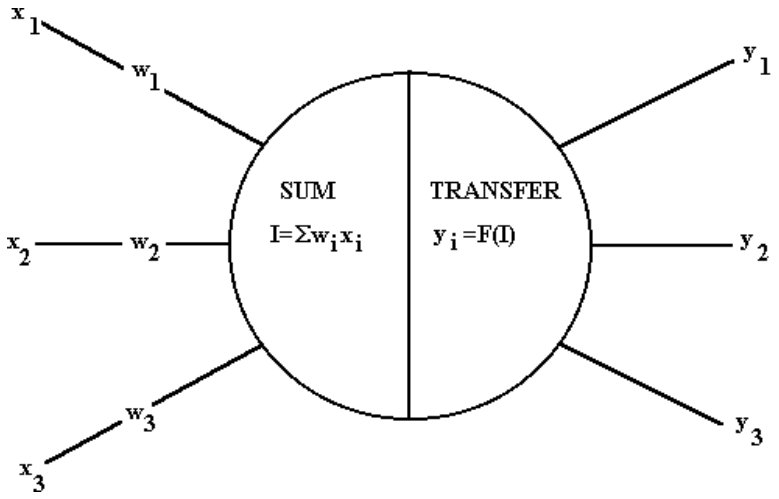

x_i - input signals y_i - output signals w_i - weights

FIGURE 1. PROCESSING ELEMENT

Nodes within a network are arranged in layers. The neural network in figure 2 consists of an input layer, a hidden or processing layer, and an output layer. The initial data enters the network through the input layer. Most of the processing takes place in the hidden layer. If the complexity of a given problem is high, more hidden layers may be required. Finally, the output layer yields the desired information.

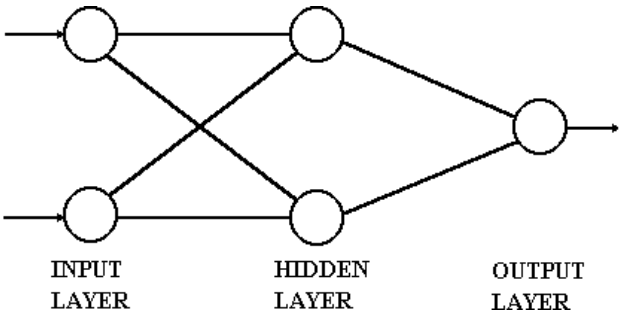

FIGURE 2. SIMPLE NEURAL NETWORK

2.3 BACKPROPAGATION NEURAL NETWORKS.

The neuron arrangement of the network shown in figure 2 is typical of the backpropagation neural network. The name “backpropagation” comes from the training method used during the learning process—back propagation of error. This training method is simply a gradient descent method that minimizes the total squared error of the output computed by the net. The very general nature of the backpropagation training method means that a backpropagation net can be

used to solve problems in many areas. It is probably the best network type to use in prediction problems such as the one addressed in this research.

2.3.1 Architecture.

A three-layer neural network with one layer of hidden units is shown in figure 3. The input neurons are denoted by "X," hidden layer neurons by "Z," and output neurons by "Y." The weights of the connections between the input and the hidden layer are denoted by "v" and the weights of the connections between the hidden and the output layer are denoted by "w." Only the direction of information flow for the feed-forward phase of operation is shown. During the backpropagation phase of learning, signals are sent in the reverse direction.

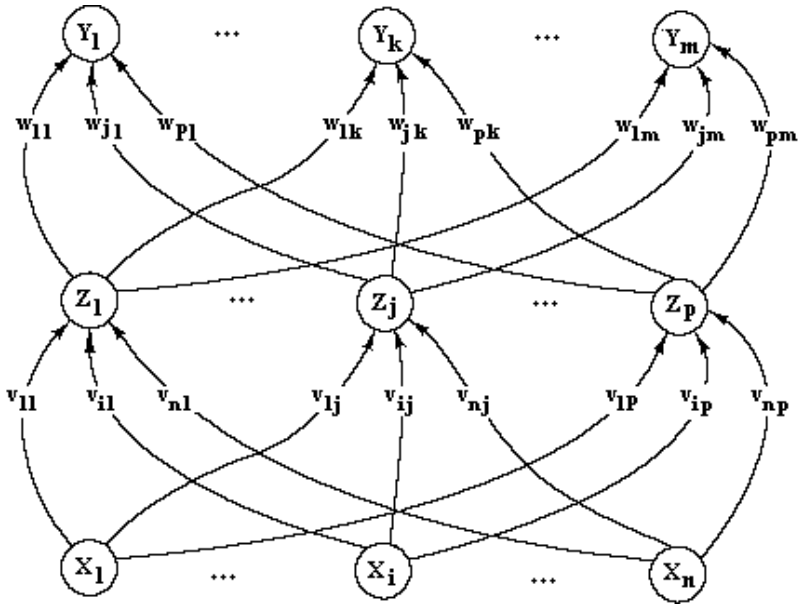

FIGURE 3. THREE-LAYER NEURAL NETWORK

Selection of the proper network architecture for the task at hand is not an exact science. Following are some general rules used to determine the initial network architecture. First, the input layer must have a number of neurons equal to the number of the input variables. In case of a prediction problem, the number of neurons in the output layer must be equal to the number of predicted variables. In the case of a classification problem, the number of neurons in the output layer must be equal to the number of possible classifications.

The number of neurons needed in the hidden layer is more difficult to establish. An arbitrary number of neurons in the hidden layer is chosen to start with. The optimum number of neurons is then found by adding or subtracting a few neurons at a time and retraining the net. Typically there is a number of hidden layer neurons that result in constant accurate predictions.

2.3.2 Activation Function.

The backpropagation net used in this study requires an activation or transfer function that is continuous, differentiable, and monotonically nondecreasing. For ease of calculations, it is desirable that the derivative be easy to compute, since it is needed for the training process. Usually, the activation function is expected to saturate, i.e., approach finite maximum and minimum values asymptotically. One of the most typical activation functions is the binary sigmoid function, which has a range of (0,1) and is defined as

$$f(x) = \frac{1}{1+e^{-x}}$$

with derivative

$$f'(x) = f(x)\left[1 - f(x)\right].$$

This function is illustrated in figure 4.

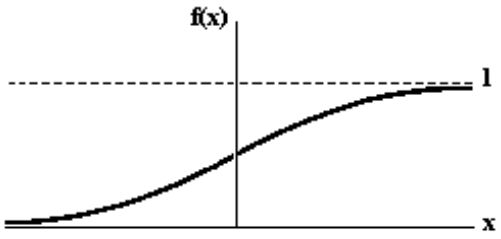

FIGURE 4. BINARY SIGMOID ACTIVATION FUNCTION

Another common activation function is the hyperbolic tangent, which has a range of (-1,1) and is defined as

$$f(x) = \frac{e^{x} - e^{-x}}{e^{x} + e^{-x}}$$

with derivative

$$f'(x) = \left(\frac{2}{e^{x} + e^{-x}}\right)^{2}$$

This function is illustrated in figure 5.

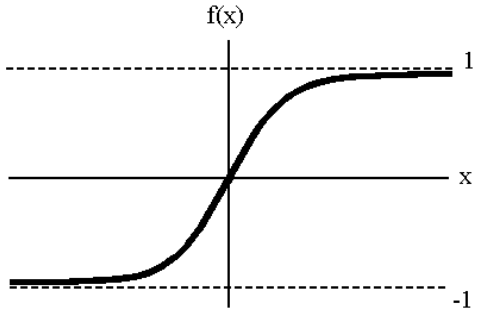

FIGURE 5. HYPERBOLIC TANGENT ACTIVATION FUNCTION

2.3.3 Training Algorithm.

Backpropagation neural networks require supervised training. Training of a network by backpropagation involves three stages: (1) feed-forward of the input training pattern, (2) backpropagation of the associated error, and (3) adjustment of the weights. During feed-forward, each input neuron (X_i) receives an input signal (x_i) and broadcasts this signal to each of the hidden layer neurons (Z_1,..., Z_p). Each hidden layer neuron then computes its activation (z_j) and sends its signal to each output neuron. The activation is computed according to the following equation:

$$z_j = f\left(\Sigma_{i=1}^{n} x_i v_{ij}\right)$$

Each output neuron (Y_k) computes its activation (y_k) to form the response of the net for the given input pattern using the equation

$$y_k = f\left(\Sigma_{j=1}^{p} z_j w_{jk}\right)$$

Each output neuron then compares its computed activation with its target value (t_k , k =1,...,m) to determine the associated error for that pattern with that unit. Based on this error, the factor δ_k is computed for each of the output neurons (Y_k). This factor is calculated using the following equation:

$$\delta_k = \left(t_k - y_k\right) f'\left(\sum_{i-1}^{p} z_j w_{jk}\right)$$

This factor is used to distribute the error at each output neuron back to all neurons in the previous layer that are connected to it. It is also used to update the weights of the connections between the hidden and the output layers. Once the error is distributed to each of the hidden layer neurons, a similar factor δ_j (j=1,..., p) is computed for each neuron in the hidden layer (Z_j) using the expression:

$$\delta = \left(\sum_{k=1}^{m} \delta_k w_{jk}\right) f'\left(\sum_{i=1}^{n} x_i v_{ij}\right)$$

It is not necessary to propagate the error back to the input layer, but this δ_j is used to update the weights between the hidden and the input layer.

After all of the δ factors have been determined, the weights for all layers are adjusted simultaneously. The adjustment to the weight w_{jk} (from hidden unit Z_j to output unit Y_k) – Δw_{jk} – is based on the factor δ_k and the activation value of the hidden unit Z_j

$$\Delta w_{jk} = \alpha \delta_k z_j$$

The adjustment to the weight v_{ij} (from input unit X_i to hidden unit Z_j) – Δv_{ij} – is based on the factor δ_j and the activation value of the input unit X_i

$$\Delta v_{ij} = \alpha \delta_j x_i$$

When all the weights have been adjusted, the above process begins again with another feed-forward phase and a new set of input signals (X_i).

The variable α is an operator-selected learning rate of the network. It is determined before the start of the training cycle. Its value ranges from 0 to 1. The learning rate affects the duration of the training process. Small values of α will result in the network taking more time to train; on the other hand, a small α is not likely to cause the network to overshoot the solution. Large values of α will cause the network to train more quickly but it might cause it to oscillate about the true solution and prevent convergence.

Aside from selection of the learning rate, other decisions must be made before the training commences. First, initial values of the weights must be determined. The values for the initial weights must not be too large, or the initial input signals to each hidden or output unit will be likely to fall in the saturation region of the sigmoid function where the derivative of the activation function is very small. If the initial weights are too small, the net input to a hidden or output unit will be close to zero. In both of these instances the learning is extremely slow. To avoid these problems, a common procedure is to initialize each weight to a random value between -0.5 and 0.5 (between -1 and 1, 0 and 1 or some other suitable interval depending upon the activation function). The value may be positive or negative because the final weights after training may also be of either sign.

Second, a training data set is needed. The training data set consists of a number of training pairs, each of which is comprised of a network input and the expected output. The training set must be a representative sample of the data that a given network is expected to process after the training cycle is finished. This means that the training set must be large enough, (i.e., it must have a sufficiently large number of training pairs) and it must cover the full range of the expected inputs and outputs.

Currently, there is no easy way of determining how many training pairs are needed for a given problem. For a classification problem, the following rule of thumb may be used.

$$P = \frac{W}{e}$$

where P is the number of training pairs required, W is the total number of weights within the network, and e is the expected error expressed as a fraction of 1. For example, with $e = 0.1$, a net with 80 weights will require 800 training pairs to ensure 90% accuracy in classifying test patterns. This rule of thumb works fairly well for classification problems. However, there is no way of determining a similar value for expected error, e, for a prediction problem. Some trial and error is required in this instance. A number of training pairs is selected and the net is trained. If it fails to train properly, the number of training pairs is increased.

The problem of covering the full range of expected inputs and outputs is somewhat easier to solve. Simply, care must be taken that a training data set covers all possible values of inputs and outputs. This is especially important in the case of a prediction problem. If certain ranges of inputs and outputs are not sufficiently represented in the training set then the network will not learn to predict these values correctly.

The final question that must be answered is how long to train the net. The purpose of training a network by backpropagation is to achieve a balance between correct responses to training patterns and good responses to new input patterns, i.e., a balance between memorization and generalization. If a net is not trained long enough it will not be able to correctly classify any patterns or predict any values. If a net is trained too long, it will begin to memorize the training data. Its performance will continue to improve for the training set, but it will perform poorly for any data that it was not exposed to during the learning cycle.

The problem of the length of the training cycle cannot be successfully addressed before the training begins. Performance of the net must be periodically evaluated during the training for both the training set and a testing set that is completely separate from the training data. As long as the performance for the testing set improves, the training continues. When the performance starts degrading, the training process is terminated. At this point the weights are frozen at their current values.

3. EXPERIMENTAL APPARATUS AND TESTING PROCEDURE.

3.1 EXPERIMENTAL APPARATUS.

A specially instrumented Cessna 172P aircraft was used to collect the flight load data. Figure 6 shows the locations of the sensors and the data acquisition system in the aircraft.

Two Columbia Research Model 2681 strain sensors were located on the front spar of the left horizontal stabilizer and two on the front spar of the vertical fin. The strain sensors were temperature compensated to account for the changes in temperature expected with altitude.

Two Columbia Research SA-107BHP linear accelerometers were mounted to the tail cone bulkhead to measure the acceleration in the vicinity of the empennage. One of the sensors was mounted with its sensing axis aligned along the aircraft y axis and the other along the aircraft z axis. The remaining two linear accelerometers (same type) were located in the cabin of the aircraft to measure acceleration in the vicinity of the aircraft c.g. These two accelerometers were installed similarly to the ones in the tail cone—one along the aircraft y axis and one along the aircraft z axis.

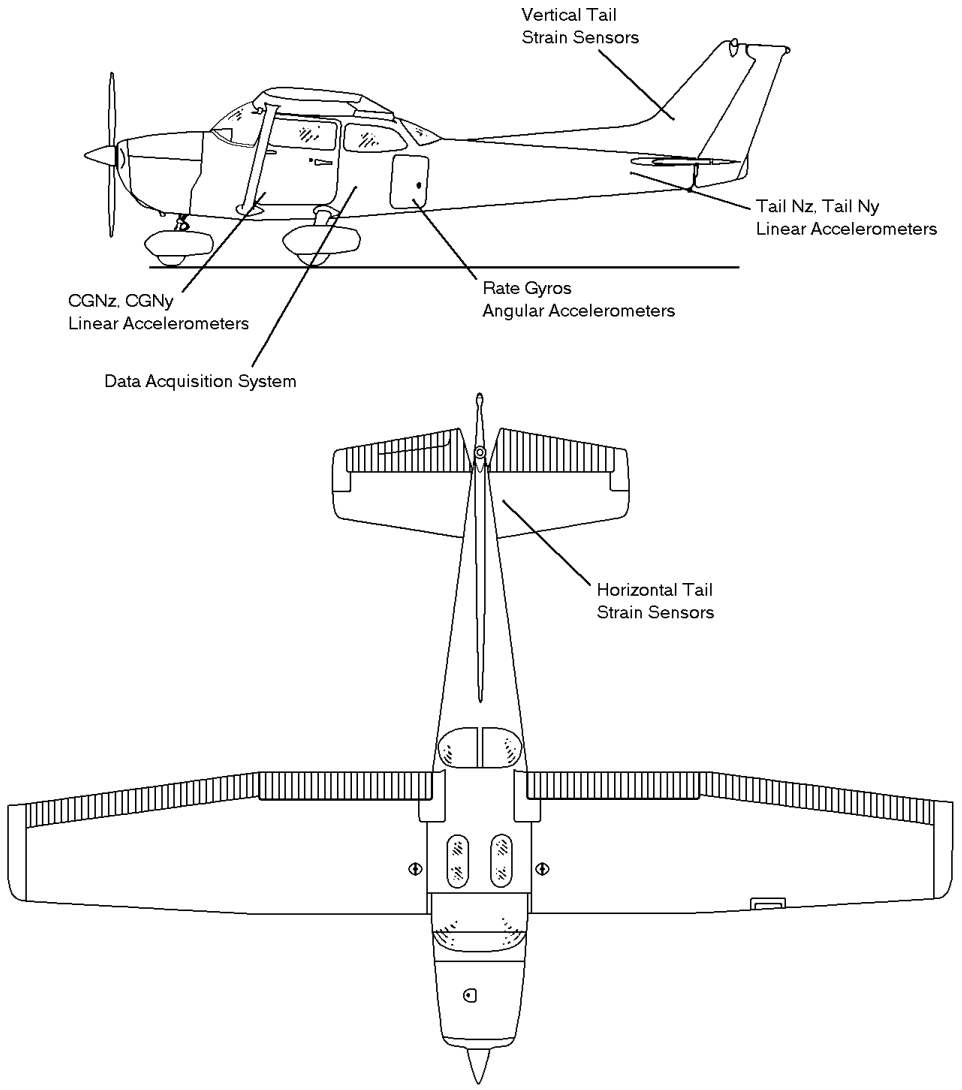

FIGURE 6. LOCATION OF THE SENSORS AND THE DATA ACQUISITION SYSTEM

Three Murata Gyrostar ENV-05H-02 solid-state rate gyros and three Shaevitz angular accelerometers were installed in the baggage compartment on a removable instrument pallet. One-rate gyro and one-angular accelerometer were provided for each of the aircraft major axes: x, y, and z.

Aside from the rate gyros and the angular accelerometers, all the other sensors were already installed on the airplane when these research efforts were begun. The rate gyros and the angular accelerometers were added to provide a more direct measurement of the necessary kinematic variables, since earlier investigations for this project showed that exclusive use of the linear accelerometers was not sufficient to predict the empennage flight loads with the desired accuracy. These kinematic variables were used as inputs for the neural networks.

The signals from all sensors were collected by an IOTech DaqBook 216 portable data acquisition system. This is a 16-bit digital data acquisition system capable of handling up to 256 input channels at 100 kHz (due to some peculiarities of the aircraft environment and the laptop PC used, 200 Hz was the actual maximum sampling rate possible). The DaqBook 216 was equipped with an IOTech DBK 15 universal current/voltage input card and an IOTech DBK43 strain gage module. The DBK 15 card was used to collect the linear accelerometer, rate gyro, and the angular accelerometer signals, while the DBK 43 card collected data from the strain gages. A portable computer was used to record the data during flight. Both the data acquisition system and the portable computer were placed on the rear passenger seat. Table 1 summarizes the hardware used to collect the data.

TABLE 1. SENSORS AND DATA ACQUISITION EQUIPMENT

Type	Model	Manufacturer	Quantity
Strain Sensor	Columbia Research Model 2681	Columbia Research Laboratories, Inc.	4
Linear Accelerometer	Columbia Research SA-107BHP	Columbia Research Laboratories, Inc.	4
Rate Gyro	Gyrostar ENV-05H-02	Murata Mfg. Co. Ltd.	3
Angular Accelerometer	Shaevitz, Inc.	Shaevitz, Inc.	3
Portable Computer	IBM PC compatible 486DX-33	Midwest Micro, Inc.	1
Portable Data Acquisition System	DaqBook 216	IOTech, Inc.	1

3.2 TESTING PROCEDURE.

The data were acquired in-flight from a series of maneuvers performed at an altitude of 3,000 ft. One-g level flight was chosen for the baseline, and the strain sensors were adjusted to output 0.0V for this condition. Sensor readings were recorded for the following maneuvers:

- Sideslip Left
- Sideslip Right
- Stabilized-g Turn Left
- Stabilized-g Turn Right

- Push-Pull
- Roll
- Dutch Roll

Each maneuver was performed once at 65 KIAS, 80 KIAS, and 95 KIAS. A maximum load factor of 3.0 was reached during a push-pull maneuver. The maneuvers and the speeds at which they were performed were chosen to cover the full range of aircraft motion and a sizable portion of its flight envelope. The part of the flight envelope that was covered (shown in figure 7) was judged to be sufficient to establish a method of strain prediction. As a result, and to assure flight test crew safety, the full-flight envelope was not explored. Appendix A describes analytical methods for estimating loads outside the flight envelope.

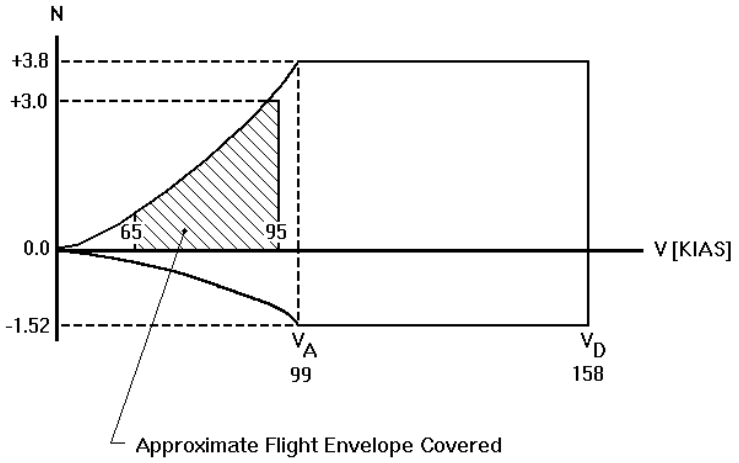

FIGURE 7. APPROXIMATE FLIGHT ENVELOPE COVERED

One data set consisted of 21 separate files—3 for each of the selected 7 maneuvers. Two data sets were recorded, one intended for the training of the neural networks and one for the testing. These two data sets were recorded on two different days in order to provide differing flight conditions.

Figure 8 shows the procedure used to collect the data for a single maneuver. First, the IOTech data acquisition system, the portable computer, and the sensors were powered up. Then *DAQView*, a software package used to control the data acquisition system, was started. Within this software a real-time input channel monitor was activated to verify that the computer properly received all signals. To record the signals from a single maneuver, the data acquisition system was set to collect 6,000 records at 200 samples per second—30 seconds (2.5 Mbytes) of data. When the typical flight profile data was collected, the data acquisition system was set to acquire 60,000 records at 200 Hz—5 minutes (25 Mbytes) of data.

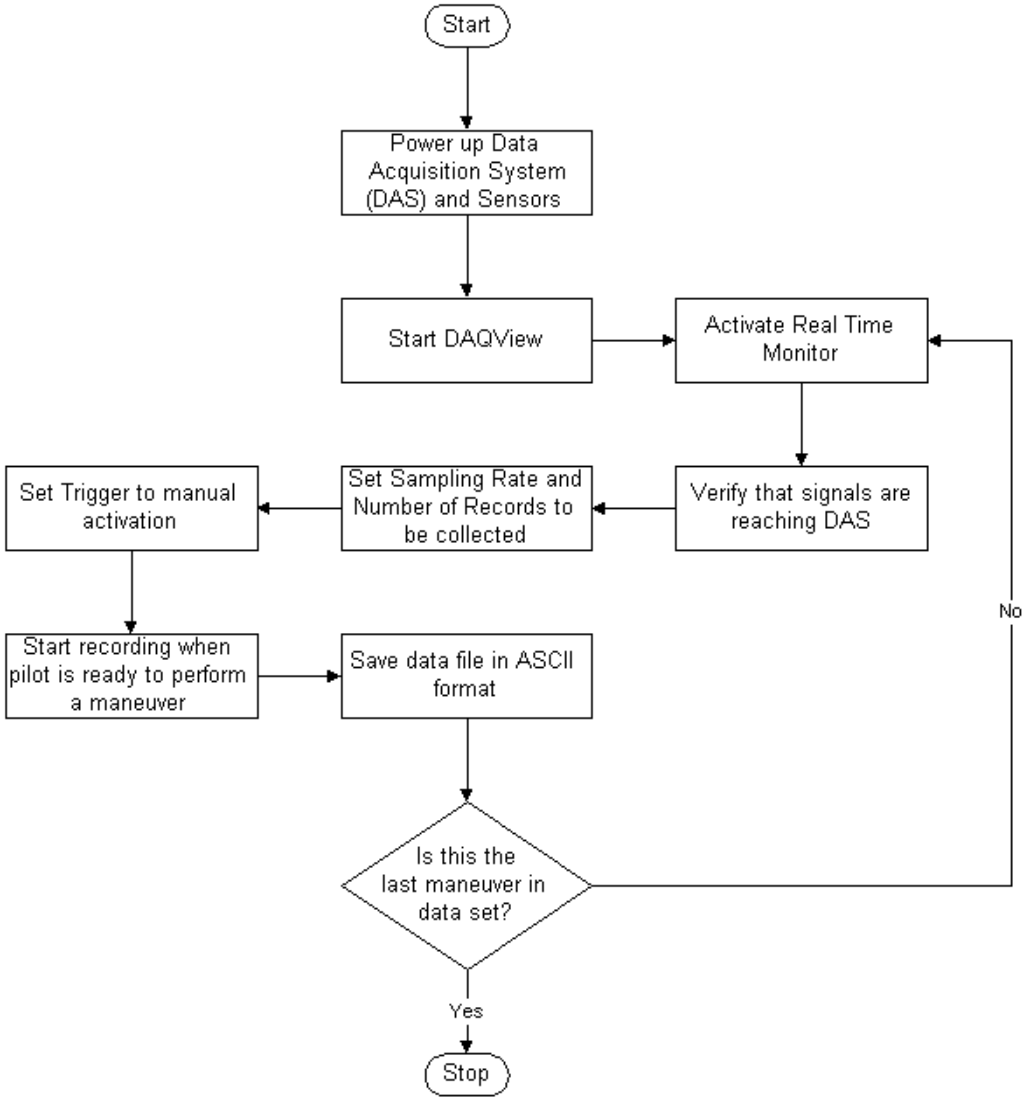

FIGURE 8. PROCEDURE USED TO COLLECT EACH MANEUVER DATA FILE

The trigger was set to manual activation, and the pilot was instructed to prepare to perform a maneuver. When the pilot was ready, the data acquisition system was triggered and the data were recorded to a binary file. After the recording was complete, the controlling software automatically converted it to ASCII format. Given that there were no problems while the signals were being recorded, this procedure was then repeated for a different maneuver.

3.3 POSTPROCESSING.

From the beginning, it was noted that there was a low signal to noise ratio in the raw data. Preliminary, neural network results indicated that the prediction accuracy improved when the raw data were filtered prior to training the network. A frequency spectrum analysis was performed using *DADisp 4.0* [8]. It indicated that the signals resulting from the pilot control inputs had frequencies of 1.5 Hz or less. Therefore, a low pass filter with a 2 Hz cutoff frequency was

designed within *DADisp*. It was noted that this filter could not properly process the first and last 50 or so records in each file. Since each maneuver began a short time after the data acquisition system was triggered and stopped before the 30-second interval ended, the first 100 and the last 99 records of each raw data file (total of about 1 second of data) were discarded with no substantial loss of information.

The typical flight data file proved too large to be handled by *DADisp* in one piece. In order to filter it, this file had to be broken up into 16 segments. Each segment was filtered and the unusable records were discarded, segment by segment, each separately. This reduced the number of records from 60,000 in the original typical flight data file to 56,816 total in all 16 parts, after which the data were ready to be used in the neural networks.

4. NEURAL NETWORK SELECTION AND IMPLEMENTATION.

4.1 SELECTION OF A NEURAL NETWORK.

4.1.1 Input Data for the Neural Network.

The two sets of the filtered data files formed the pool of possible inputs for the neural networks. Of the two data sets, one was used for training and the other was reserved for testing.

It was assumed that two networks were necessary to predict strain in the empennage structure; one for the horizontal tail and one for the vertical tail. Thus, before the neural network training began, the available signals were tentatively split up into two groups. The first group contained the signals that were thought to be useful in the prediction of the strain in the horizontal tail.

- c.g. Nz
- Tail Nz
- Pitch rate
- Yaw rate
- Pitch acceleration
- Yaw acceleration
- Roll acceleration
- Roll rate
-

The second group included only the signals that were assumed to be helpful in the prediction of the strain in the vertical tail:

- c.g. Ny
- Tail Ny
- Roll rate
- Roll acceleration
- Yaw acceleration
- Rate yaw Rate

In order for the neural networks to properly learn the relationship between the strains and the kinematic variables, the full range of measured strains had to be represented within the training files. Table 2 shows the strains measured in flight for each maneuver. It should be noted that since the strain sensors were zeroed at the 1-g flight condition, zero strain meant that there was no variation from this flight condition and not that the strain was actually zero.

TABLE 2. MAXIMUM AND MINIMUM STRAINS OBSERVED FOR EACH MANEUVER

	Vertical Tail		Horizontal Tail	
Maneuver	Max. Strain με	Min. Strain με	Max. Strain με	Min. Strain με
Dutch Roll	165	-178	112	-131
Roll	29	-119	95	-160
Sideslip Left	4	-92	26	-98
Sideslip Right	17	-68	82	-59
Stabilized-g Turn Left	14	-69	17	-63
Stabilized-g Turn Right	4	-71	32	-67
Push-Pull	-5	-61	44	-97

As shown in table 2, the maximum strain in both the horizontal tail and the vertical tail occurred during the dutch-roll maneuver.

4.1.2 Neural Network Architecture.

The choice of a neural network type was driven by the fact that the relationship between the kinematic variables and the strain was unknown and that there was no guarantee that this relationship remained constant throughout the test flight envelope. A modular neural network (MNN) was chosen to handle this problem [9]. A MNN may be thought of as a generalization of a backpropagation neural network. It consists of a group of neural networks—referred to as local experts—competing to learn different aspects of a problem. A gating network controls the competition and learns to assign different regions of the data space to different local expert networks. Thus, if the relationship between the strain and the kinematic variables changed from one maneuver to another or from one speed to another, the neural network would still be able to learn to predict strain at all flight conditions. Sample architecture of a modular neural network is shown in figure 9.

Both the gating network and the local experts have full connections from the input layer. The gating network has as many output nodes as there are local experts. Training occurs simultaneously for the gating network and for the local experts. Competition among the local experts is encouraged, so that, for a given input vector, the gating network will tend to choose a single local expert rather than a mixture of them. In this way, the input space is automatically partitioned into regions and each local expert takes responsibility for a different region.

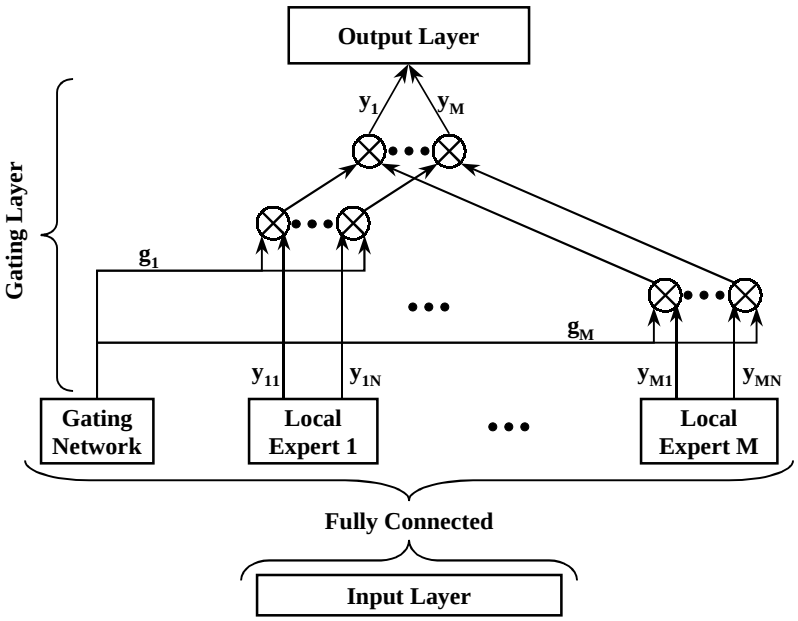

FIGURE 9. GENERAL ARCHITECTURE OF A MODULAR NEURAL NETWORK

4.2 NEURAL NETWORK IMPLEMENTATION.

4.2.1 Selection of Controlling Parameters.

All of the neural networks created in the course of this research were formed, trained, and tested using the *NeuralWorks Professional II/Plus* version 5.20 software [10]. The program is capable of automatically generating a modular neural network from the specified parameters. The parameters of the networks selected are listed in table 3. Unless otherwise noted, these parameters are the same for both the horizontal and the vertical tail networks.

TABLE 3. PARAMETERS OF THE MODULAR NEURAL NETWORKS

Number of Inputs	Dependent on the Combination of Signals Used for Input
Local Expert Hidden Layer Neurons	30
Local Expert Output Layer Neurons	1
Gating Network Hidden Layer Neurons	400
Gating Network Output Layer Neurons	5
Learning Rule	Extended Delta-Bar-Delta (EDBD)
Transfer Function	TANH
Epoch	Vertical Tail Network: 20 Horizontal Tail Network: 15
F' Offset	0.3

In the search for the best signals to use for training of the neural networks, the number of input layer neurons varied from 2 to 6 as various combinations of inputs were tried out. The number of neurons in the hidden layer of each local expert was arbitrarily set to 30. During initial testing, this number was increased to as high as 50 with no appreciable change in network performance. All local experts had a single neuron in their output layers—this was dictated by the fact that each of these networks was expected to predict a single value—the strain in either the horizontal or the vertical tail.

The number of neurons in the hidden layer of the gating network was set to 400. Gating networks with less than 400 hidden layer neurons were tried, but the network performance decreased substantially. The number of the neurons in the output layer of the gating network (and subsequently the number of the local experts) was set to 5. This proved sufficient, as none of the subsequently trained networks required the use of more than three of the five available local experts.

The extended delta-bar-delta (EDBD) learning rule was selected. This learning rule automatically selected and adjusted the learning coefficient, learning coefficient ratio, the learning coefficient transition point, and the momentum term. This minimized the learning time and reduced the number of network parameters that had to be selected iteratively. A hyperbolic tangent transfer function was appropriate for the problem at hand because the input values ranged from -1 to +1.

The epoch sets the number of training pairs that are presented to the network before the weights are updated. Larger and smaller epochs were tried for both networks, which resulted in generally worsened network performance.

The F' offset is a constant added to the value of the derivative of the neuron activation function during training in order to prevent neuron saturation. The *NeuralWorks* Users Guide suggests that it be set to 0.3 for the hyperbolic tangent activation function. F' offsets of 0.1 and 0.2 were also tried with no change in the results.

4.2.2 Neural Network Training.

Before the training began, two lists of possible input combinations were formed, one for the horizontal tail and one for the vertical tail. A separate training file was generated for each possible input combination. As noted earlier, the observed strain magnitudes forced the use of certain maneuvers in the training files. Thus, all training files used to train horizontal tail networks contained roll, dutch-roll, and push-pull files for a total of 17,403 records. Similarly, all vertical tail network training files contained roll and dutch-roll files for a total of 11,602 records.

A neural network was formed using the Instanet utility within the *NeuralWorks* program. The operator entered all the parameters, and the software automatically generated the network architecture. The operator then selected the training file and the length of the learning cycle was

set to be equal to the number of records in the training file. The training pairs were presented to the network in random order.

4.2.3 Neural Network Testing.

After the training was completed, each maneuver data file was used to test the network. This produced 40 result files for each neural network. A BASIC program was used to calculate the maximum error between the measured and predicted strain values and the number of points falling outside of the tolerance band for each maneuver. Using the Poly Software International (Psi Plot) software package [11], scatter plots of the network results were formed.

5. ANALYSIS OF RESULTS.

5.1 EVALUATION CRITERIA.

Before the results can be evaluated, one must first establish a baseline definition of the ideal neural network output. In view of the problem at hand, the following guidelines were derived.

First, not all stresses that may be experienced by a structure significantly contribute to the accumulated fatigue damage. A stress lower than that necessary to cause failure after 10^7 cycles (for a given stress ratio) is not considered to cause fatigue damage. Thus, an insignificant stress region was defined to exist at or below 1,000 psi. According to the S-N curves for 2024 aluminum, the minimum stress that causes fatigue damage is 5,000 psi for a full stress reversal. The cutoff of 1,000 psi was selected due to the fact that the strain gages were not located at the points where the stresses were greatest and because the aircraft was not flown to all corners of its flight envelope.

Second, within the significant stress region, a tolerance band of ± 50 με was assumed. Since eventually this method is to be used to help evaluate the fatigue life of empennage structures, the stresses should be predicted at least as accurately as they are plotted on the Maximum Stress axis of the S-N curves. The stresses in the S-N curves found in the MIL-HDBK-5E are plotted to within 1,000 psi, which for aluminum translates to 100 με [12]. Thus, this number was selected as the full width of the tolerance band.

5.2 GENERAL OBSERVATIONS.

It was noted that only a small fraction of the recorded strains due to maneuver loads resulted in stresses larger than 1,000 psi. Out of 232,040 records collected, 4,332 or about 2% contained strains that produced significant horizontal tail stresses. Similarly, there were only 6,696 records—about 3%—with vertical tail strains that resulted in stresses larger than 1,000 psi.

For the horizontal tail, the significant strains were produced by the roll and dutch-roll maneuvers. All of the significant vertical tail strains were caused by the dutch rolls. It was surprising that the steady-state maneuvers (sideslip for the vertical tail and the stabilized-g turn for the horizontal tail) all resulted in very small strains. The horizontal tail strains observed during push-pulls were also surprisingly small, though not as small as those resulting from the stabilized-g maneuvers.

5.3 HORIZONTAL TAIL NEURAL NETWORK RESULTS.

The best horizontal tail strain prediction results were obtained when the x-, y-, and z-axes angular accelerometers and the c.g. Nz linear accelerometer signals from a dutch roll at 80 KIAS, a roll at 80 KIAS, and a push-pull at 80 KIAS were used to train the neural network. These results are summarized in table 4 and figures 10 through 19. Table 4 shows the number of significant strains, number of strains predicted that fell outside of the tolerance band, and the maximum error of prediction for those maneuvers that caused at least some significant stresses in the horizontal tail. Figures 10 through 19 present the results as x, y plots of the normalized predicted strain vs. the normalized measured strain. Since the neural network needed inputs that ranged from -1 to +1, the magnitudes of the signals used to train it had to be normalized to fall within this range. Zero strain means no variation from the baseline flight condition, which was a 1-g level flight. Positive values of strain correspond to a load factor less than 1.0 (strain gage in tension) and negative to a load factor greater than 1.0 (strain gage in compression).

TABLE 4. SUMMARY OF THE RESULTS OF THE HORIZONTAL TAIL STRAIN PREDICTION

	Significant Stress Region			Entire Data File		
Maneuver	Number of Records	Records Outside of Tolerance Band of 500 psi (50 με)	Maximum Error of Prediction (με)	Number of Records	Records Outside of Tolerance Band of 500 psi (50 με)	Maximum Error of Prediction (με)
Dutch Roll, 80 KIAS, Training Set	384	0	45	5,801	0	49
Dutch Roll, 95 KIAS, Training Set	184	0	32	5,801	357 (6%)	69
Dutch Roll, 80 KIAS, Testing Set	45	0	36	5,801	102 (2%)	58
Dutch Roll, 95 KIAS, Testing Set	730	202 (27%)	82	5,801	604 (10%)	82
Roll, 65 KIAS, Training Set	313	0	30	5,801	0	40
Roll, 80 KIAS, Training Set	585	0	44	5,801	0	44
Roll, 95 KIAS, Training Set	1,021	34 (3%)	55	5,801	103 (2%)	66
Roll, 65 KIAS, Testing Set	25	0	38	5,801	0	42
Roll, 80 KIAS, Testing Set	297	0	39	5,801	58 (1%)	55
Roll, 95 KIAS, Testing Set	748	54 (7%)	59	5,801	236 (4%)	63
Total	4,332	290 (7%)		232,040*	16,950 (7%)*	

*These include the maneuvers that did not result in significant strains.

The horizontal tail neural network was able to predict 93% of the significant strains to within 50 με of their corresponding measured values. It had a tendency to underestimate the magnitudes of strains resulting from the dutch-roll maneuvers as is apparent from figures 10 through 13.

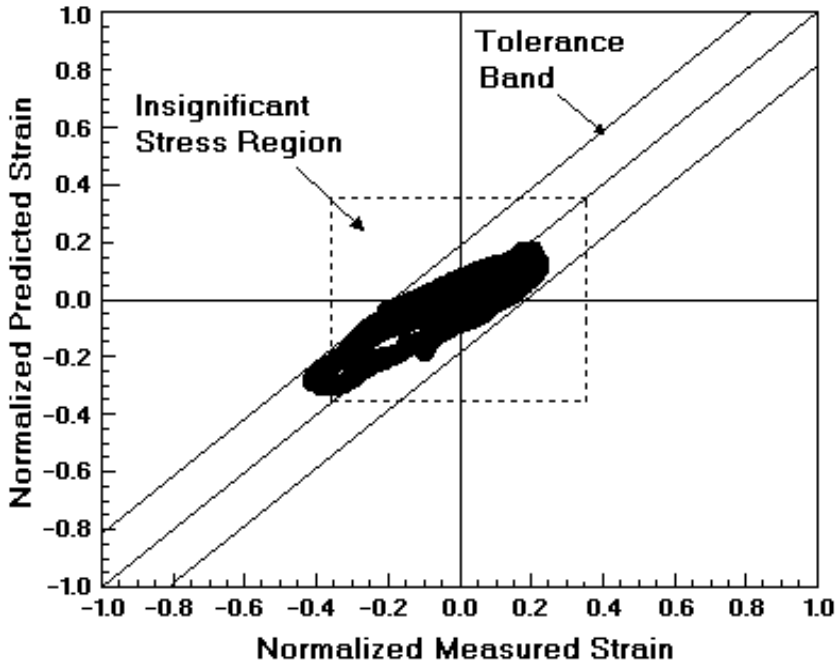

FIGURE 10. DUCTH ROLL, 80 KIAS, HORIZONTAL TAIL, TRAINING SET—
STRAIN PREDICTION RESULTS

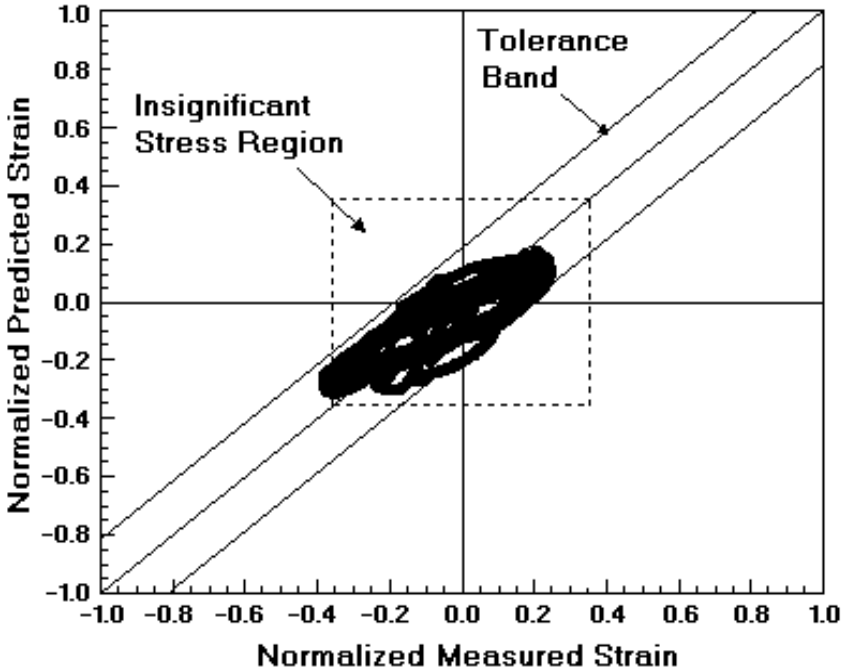

FIGURE 11. DUTCH ROLL, 80 KIAS, HORIZONTAL TAIL, TESTING SET—
STRAIN PREDICTION RESULTS

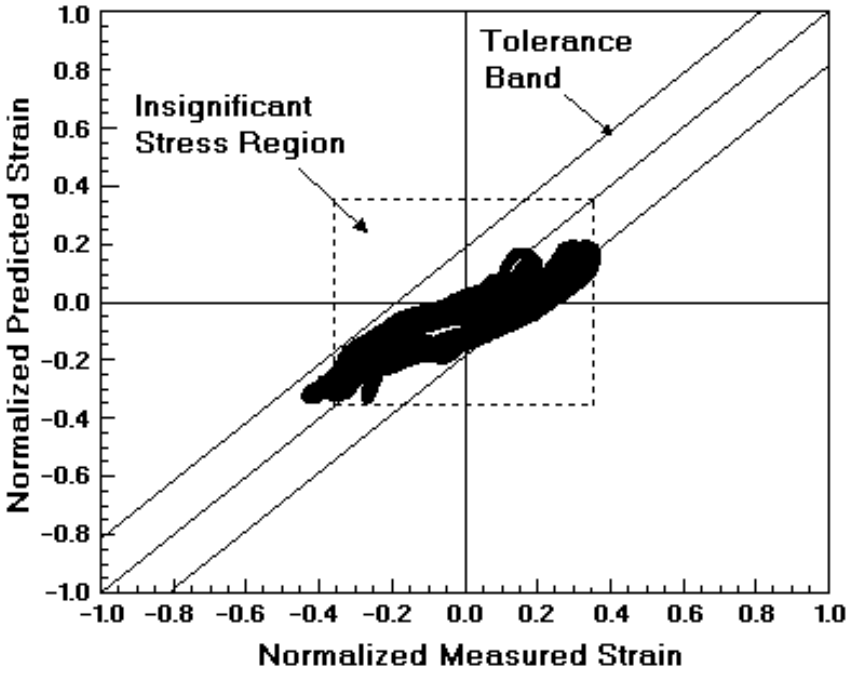

FIGURE 12. DUTCH ROLL, 95 KIAS, HORIZTONAL TAIL, TRAINING SET—
STRAIN PREDICTION RESULTS

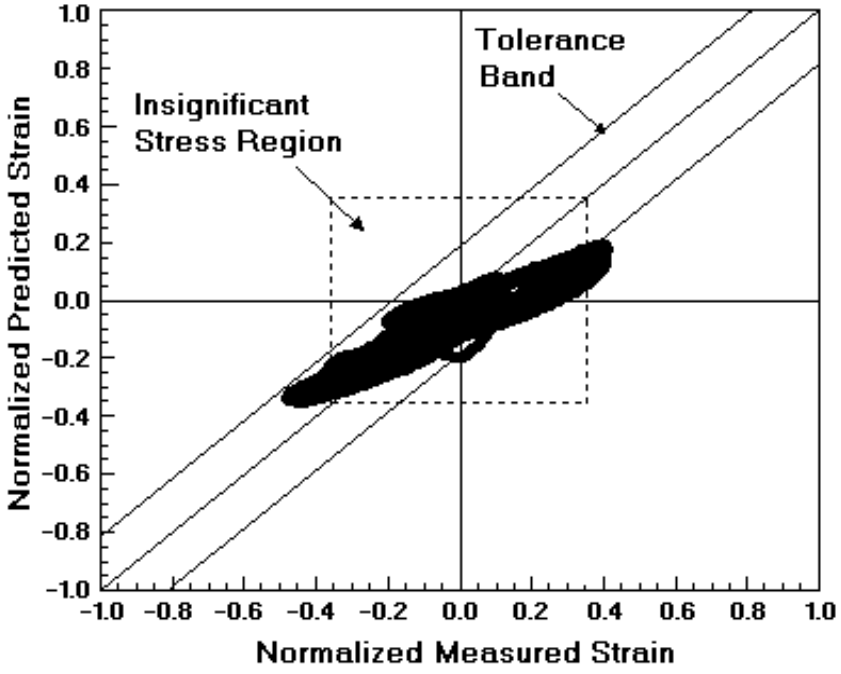

FIGURE 13. DUCTH ROLL, 95 KIAS, HORIZTONAL TAIL, TESTING SET—
STRAIN PREDICTION RESULTS

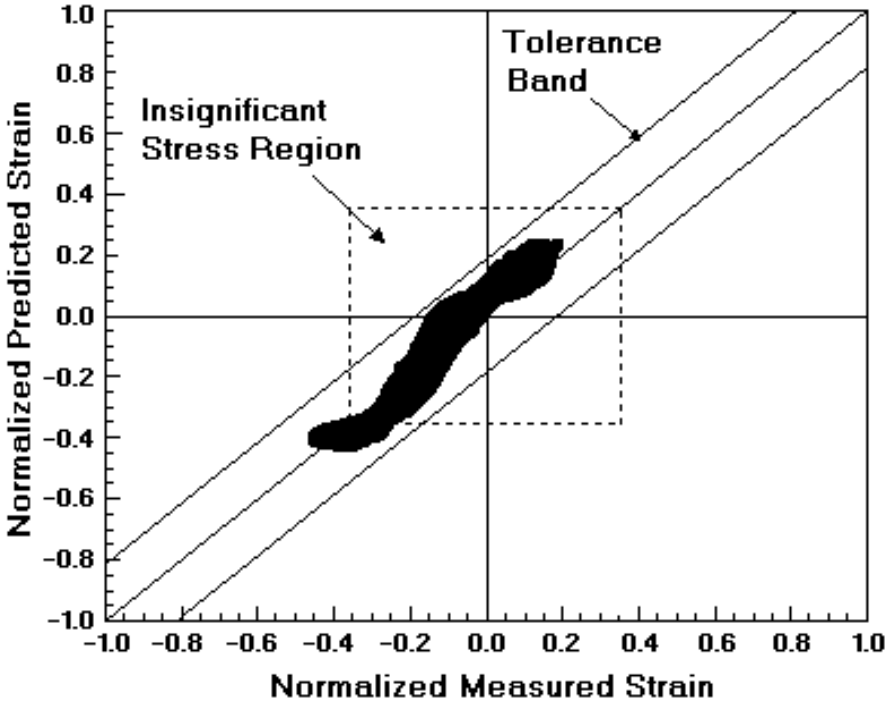

FIGURE 14. ROLL, 65 KIAS, HORIZONTAL TAIL, TRAINING SET—
STRAIN PREDICTION RESULTS

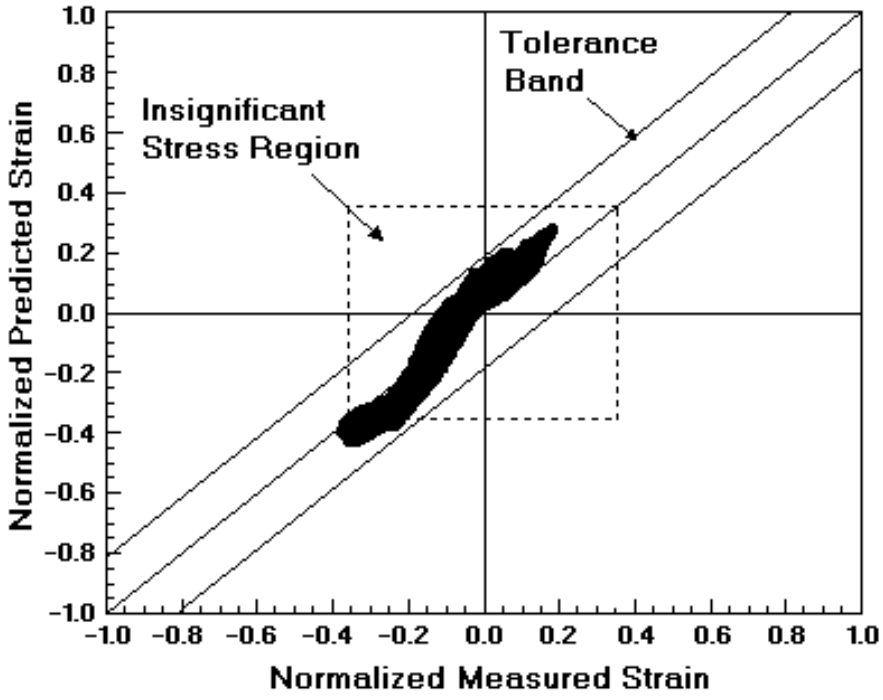

FIGURE 15. ROLL, 65 KIAS, HORIZONTAL TAIL, TESTING SET—
STRAIN PREDICTION RESULTS

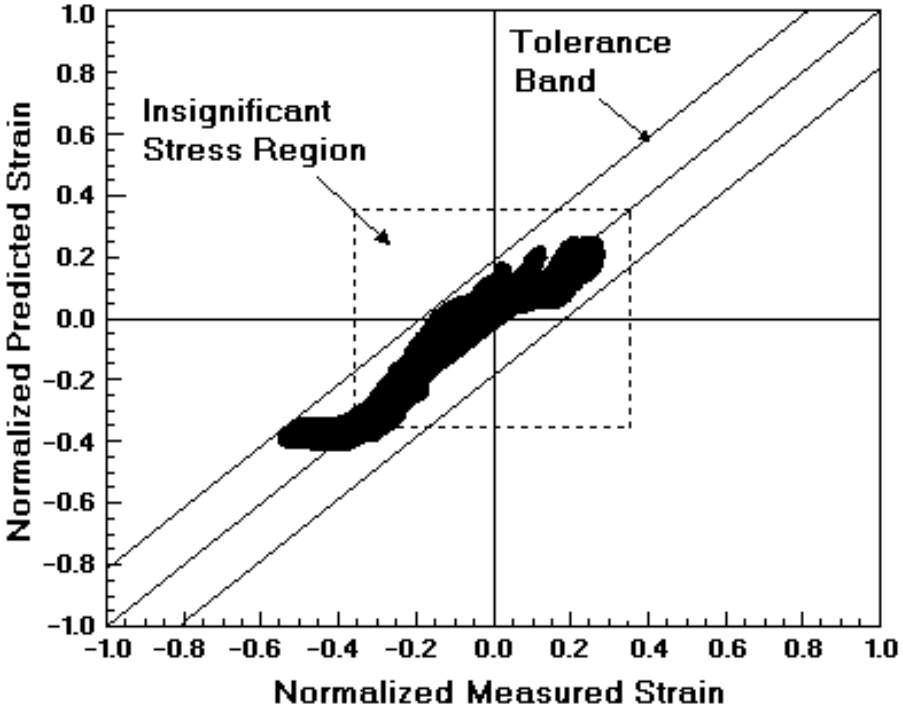

FIGURE 16. ROLL, 80 KIAS, HORIZTONAL TAIL, TRAINING SET—
STRAIN PREDICTION RESULTS

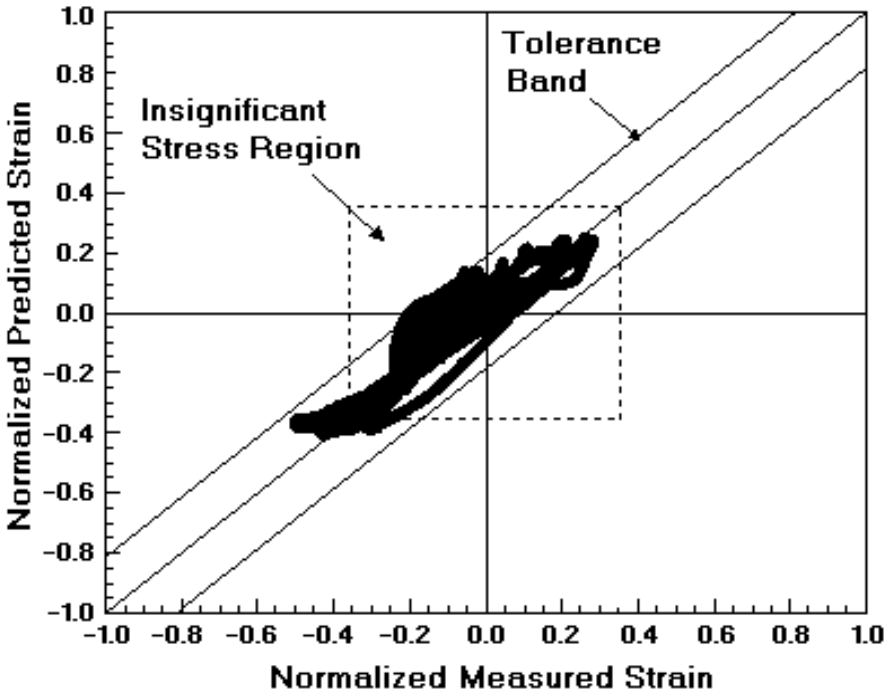

FIGURE 17. ROLL, 80 KIAS, HORIZONTAL TAIL, TESTING SET—
STRAIN PREDICTION RESULTS

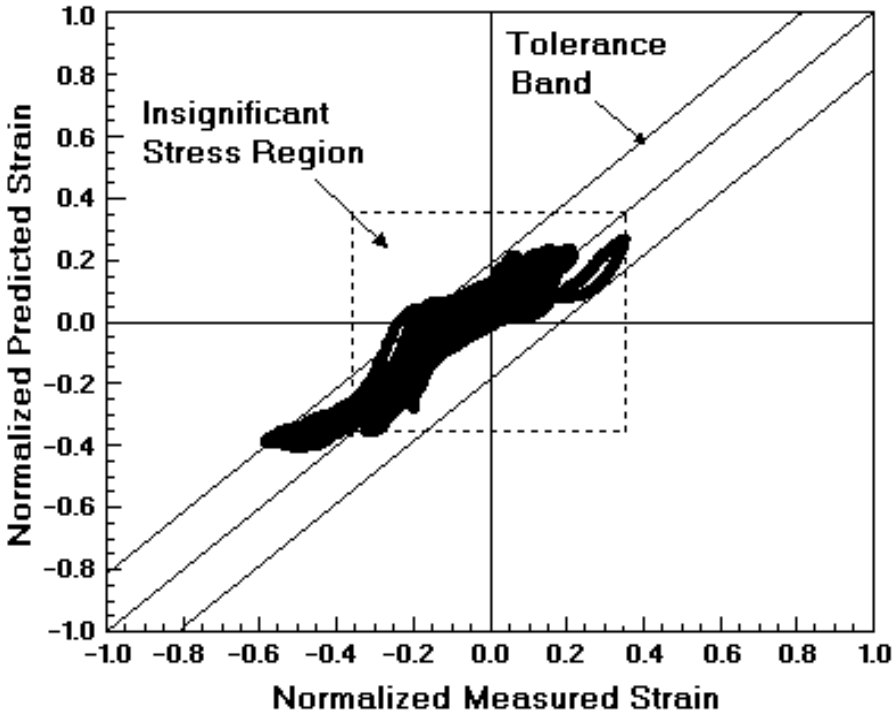

FIGURE 18. ROLL, 95 KIAS, HORIZONTAL TAIL, TRAINING SET—STRAIN PREDICTION RESULTS

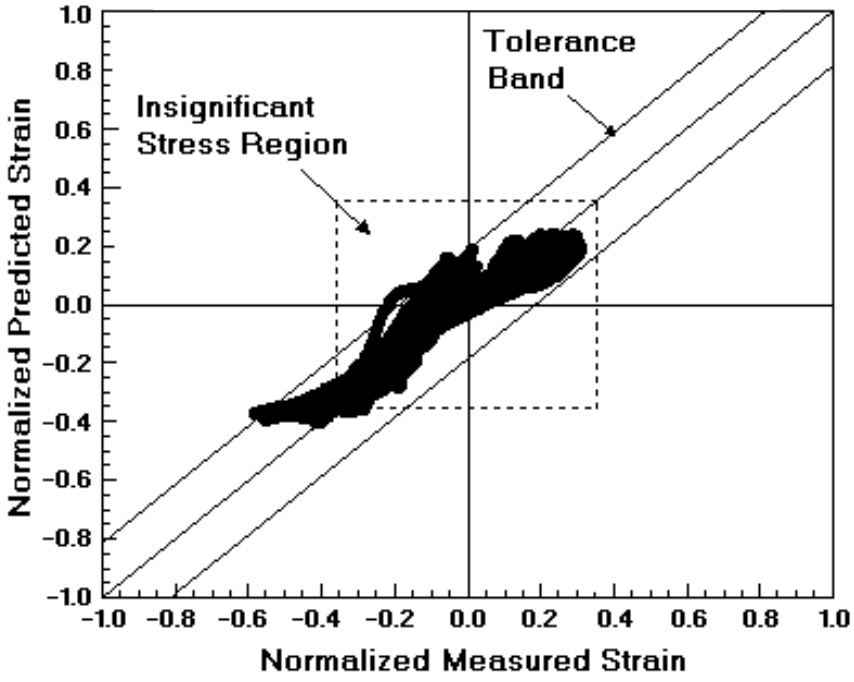

FIGURE 19. ROLL, 95 KIAS, HORIZONTAL TAIL, TESTING SET—STRAIN PREDICTION RESULTS

The strain prediction for the roll maneuver (figures 14 through 19) produced better results when the strain gage was in tension—positive normalized strain. In this region the predicted strains agreed closely with the measured strains. When the strain gage was in compression—negative normalized strain—as the strains increased, the neural network again tended to underestimate the strains.

All the strains collected from the sideslip, stabilized-g turn, and push-pull were insignificant. The neural network was able to predict these properly, i.e., for these maneuvers all the measured strains and all the predicted strains fell within the insignificant stress region.

5.4 VERTICAL TAIL NEURAL NETWORK RESULTS.

The results of the vertical tail strain prediction are summarized in table 5 and figures 20 through 27. The neural network that produced these results was trained using the y- and x-axes angular accelerometer signals collected from roll and dutch-roll maneuvers both at 80 KIAS.

TABLE 5. SUMMARY OF THE RESULTS OF THE VERTICAL TAIL STRAIN PREDICTION

Maneuver	Significant Stress Region			Entire Data File		
	Number of Records	Records Outside of Tolerance Band of 500 psi (50 με)	Max. Error of Prediction (με)	Number of Records	Records Outside of Tolerance Band of 500 psi (50 με)	Max. Error of Prediction (με)
Dutch Roll, 65 KIAS, Training Set	332	0	40	5,801	238 (4%)	51
Dutch Roll, 80 KIAS, Training Set	1,469	0	33	5,801	0	34
Dutch Roll, 95 KIAS, Training Set	1,830	0	23	5,801	0	39
Dutch Roll, 65 KIAS, Testing Set	102	0	34	5,801	158 (3%)	51
Dutch Roll, 80 KIAS, Testing Set	987	0	33	5,801	0	39
Dutch Roll, 95 KIAS, Testing Set	1,976	0	34	5,801	15 (0.3%)	42
Total	6,696	0	0	232,040*	411 (0.2%)*	

*These include the maneuvers that did not produce significant strains.

In the portion of the flight envelope covered during the data collection, the only maneuver that produced significant stresses in the vertical tail was the dutch roll. The neural network predicted 100% of the significant strains to within the predefined tolerance band. With the exception of the dutch-roll, 65 KIAS, and training set file, the maximum error of prediction in the significant stress region was equal to or less than ±40 με—smaller than the target of ±50 με. All the insignificant strains resulting from the remaining maneuvers were properly predicted.

In all cases, as the magnitude of the strain increased the accuracy of the prediction improved (figures 20 through 25). In all dutch-roll maneuvers, the largest deviation occurred in the region from -0.2 to +0.2 normalized measured strain. The strains of these magnitudes were observed when the aircraft was at bank and yaw angles close to 0 degrees. During this portion of the maneuver, the only control input was rudder deflection, and for a short time the aircraft motion was similar to a sideslip. Thus, for the strains collected in this segment of the dutch-roll, the network output was very similar to that for the sideslip maneuvers shown in figures 26 and 27.

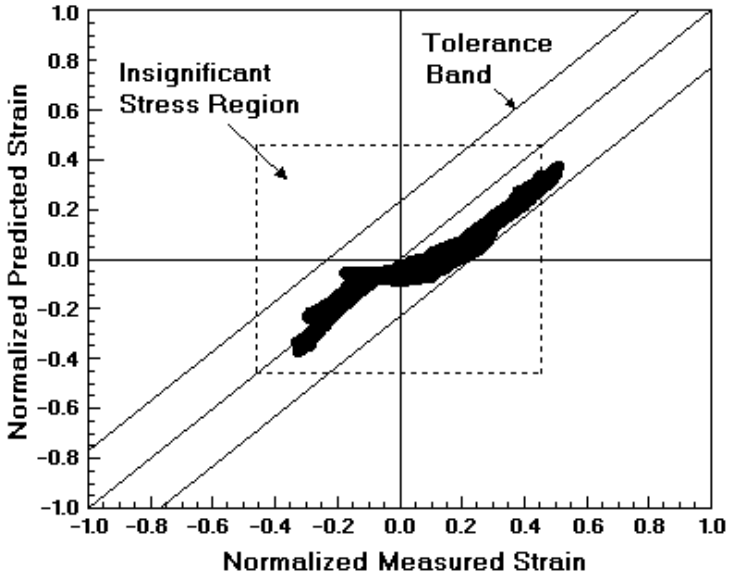

FIGURE 20. DUTCH ROLL, 65 KIAS, VERTICAL TAIL, TRAINING SET—
STRAIN PREDICTION RESULTS

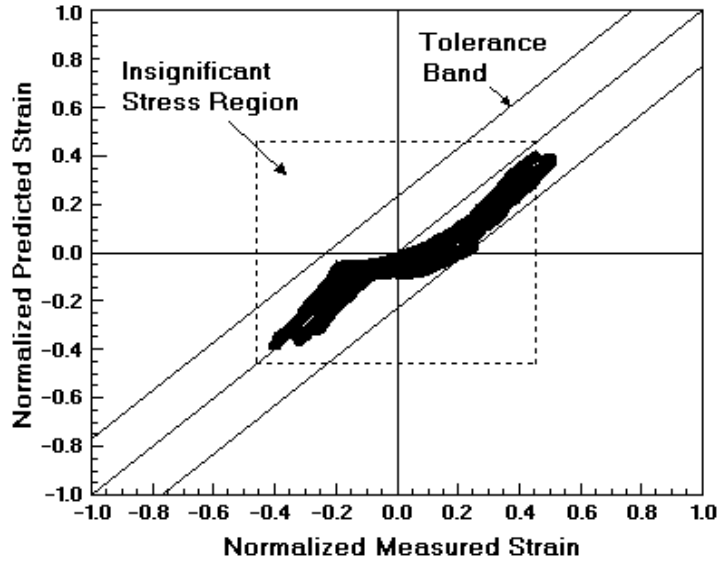

FIGURE 21. DUTCH ROLL, 65 KIAS, VERTICAL TAIL, TESTING SET—
STRAIN PREDICTION RESULTS

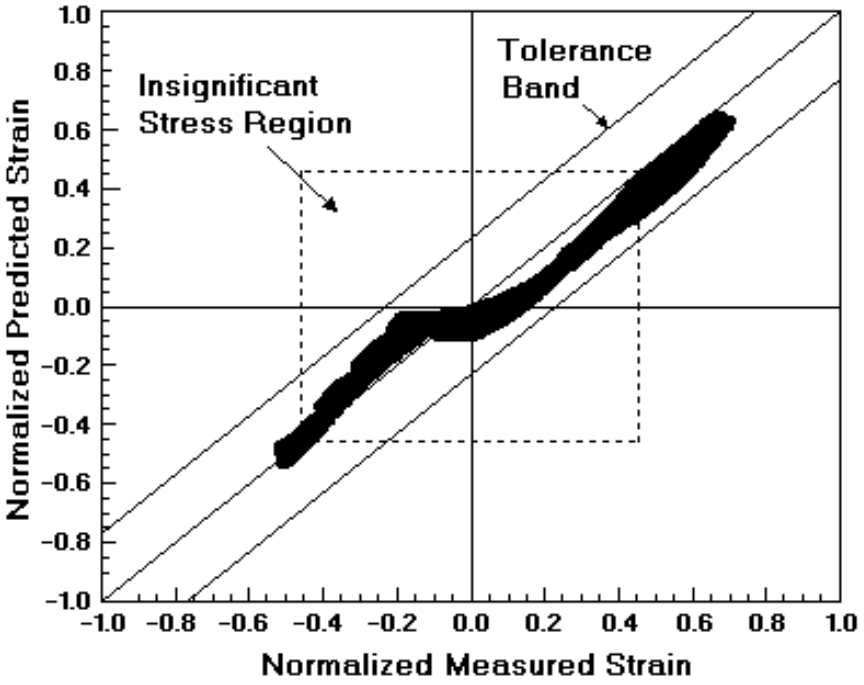

FIGURE 22. DUTCH ROLL, 80 KIAS, VERTICAL TAIL, TRAINING SET—
STRAIN PREDICTION RESULTS

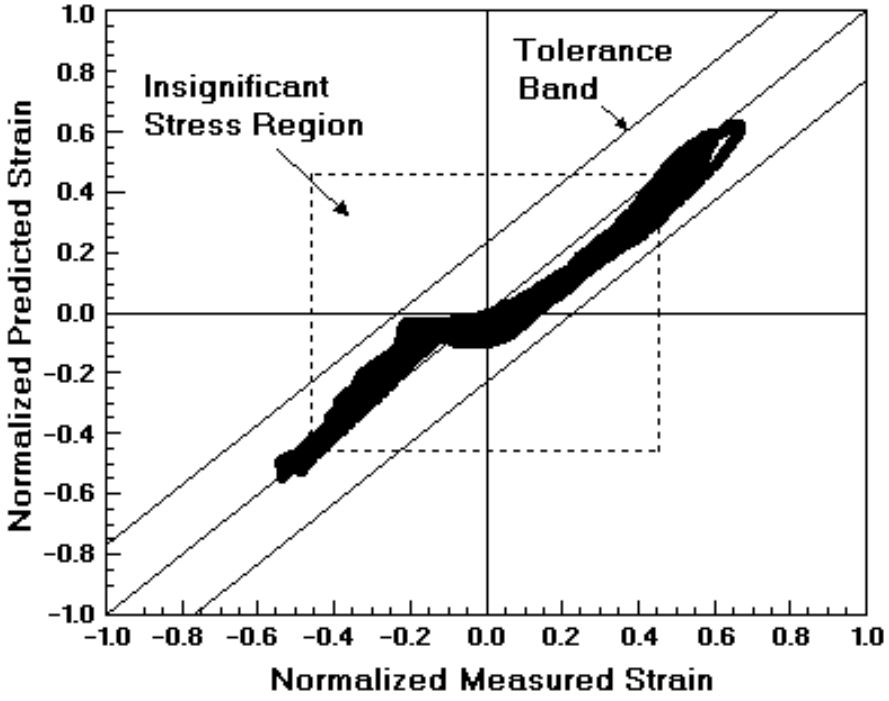

FIGURE 23. DUTCH ROLL, 80 KIAS, VERTICAL TAIL, TESTING SET—
STRAIN PREDICTION RESULTS

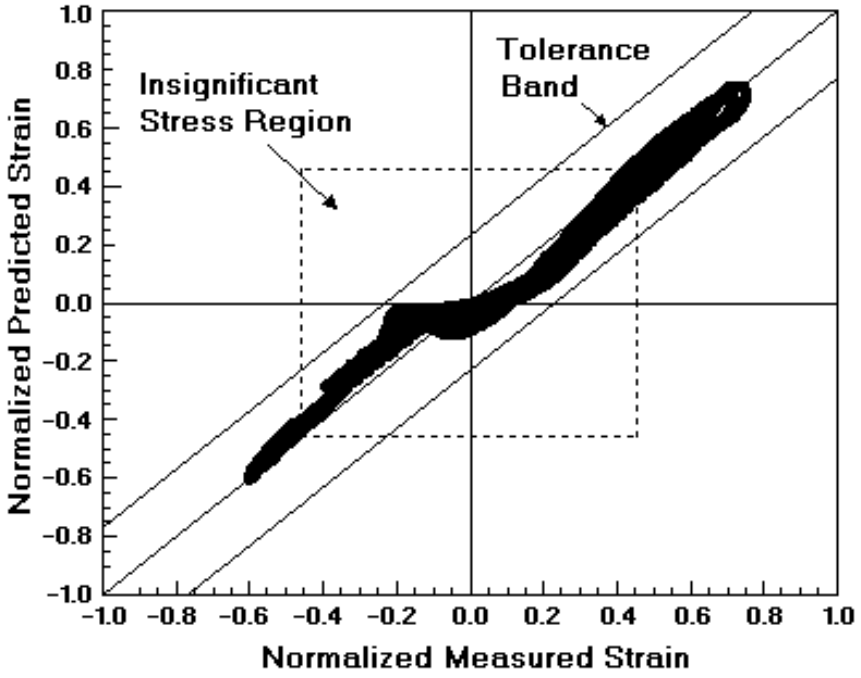

FIGURE 24. DUTCH ROLL, 95 KIAS, VERTICAL TAIL, TRAINING SET—
STRAIN PREDICTION RESULTS

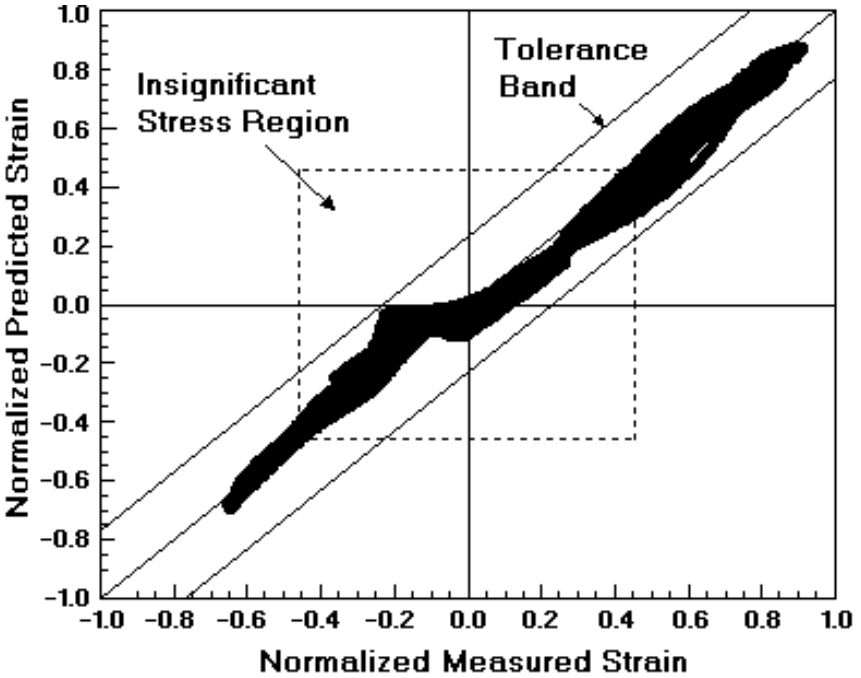

FIGURE 25. DUTCH ROLL, 95 KIAS, VERTICAL TAIL, TESTING SET—
STRAIN PREDICTION RESULTS

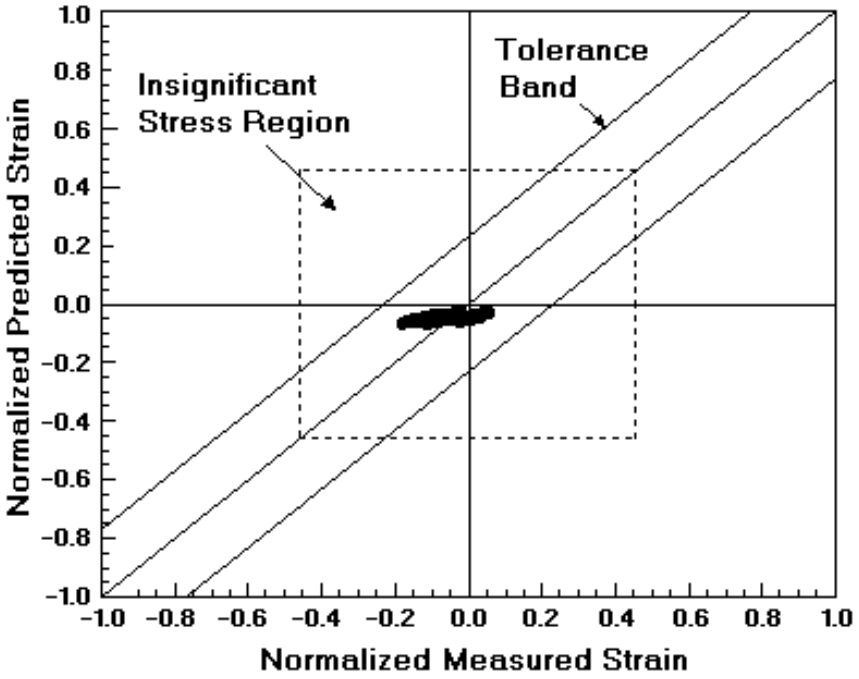

FIGURE 26. SIDESLIP LEFT, 80 KIAS, VERTICAL TAIL, TESTING SET—
STRAIN PREDICTION RESULTS

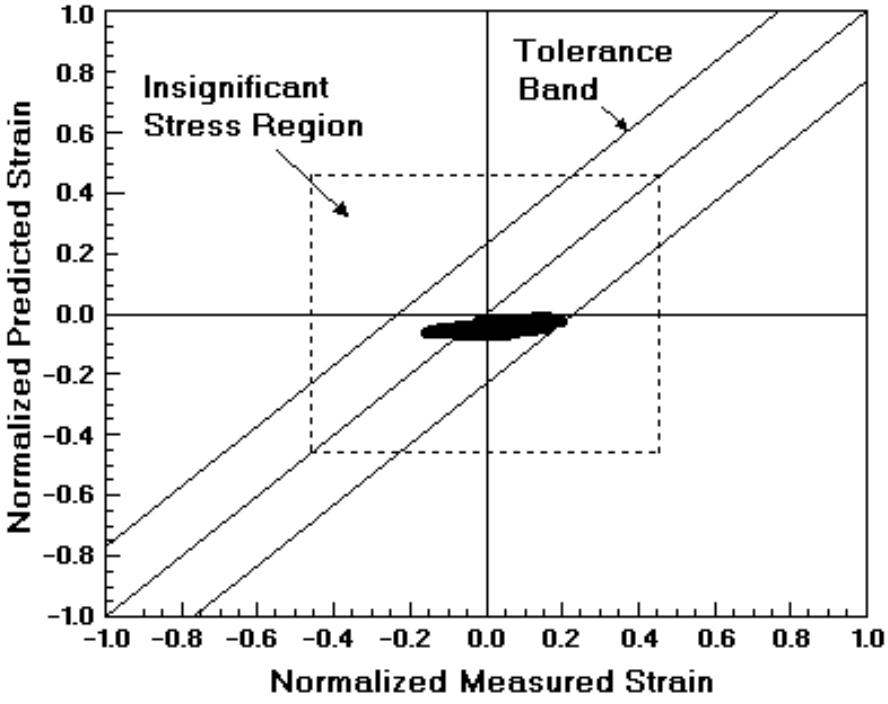

FIGURE 27. SIDESLIP RIGHT, 65 KIAS, VERTICAL TAIL, TRAINING SET—
STRAIN PREDICTION RESULTS

6. CONCLUSIONS AND RECOMMENDATIONS.

The backpropagation neural networks successfully predicted the strain from the maneuver loads in the empennage structure of a Cessna 172P within acceptable limits. For the Cessna 172P, the x-, y-, and z-axis angular accelerometer and c.g. Nz linear accelerometer signals were sufficient to train the neural networks that were used to predict the strains in the maneuver loads. The x-, y-, and z-axis angular accelerometers and the c.g. Nz linear accelerometer appear to be the minimum set of sensors required to predict the strains in the horizontal and the vertical tail of a Cessna 172P. While not as accurate as direct measurement using strain gages, the remote sensors and the neural networks are adequate for flight load measurements to establish the fatigue loads spectra database. For the maneuvers performed, the empennage flight loads were small.

Both the horizontal and the vertical tail neural networks used angular accelerometer signals. Present day angular accelerometers of the type used herein cost between $1,700 to $3,000. In order to reduce the price of the instrumentation, the rate gyro signals were numerically differentiated to obtain angular accelerations. These derived angular acceleration signals should be used instead of the raw angular accelerations to train the neural networks. Should these new networks be equally capable of accurately predicting the strains, the cost of the instrumentation would be significantly reduced as the rate gyros cost only $300 each.

The neural networks developed in the course of this research—especially the horizontal tail neural network—should be optimized to reduce the amount of time necessary to calculate the strains and, if necessary, to improve the accuracy of the prediction. An effort should also be made to determine if there is a better way of presenting data to the neural networks. In the current neural networks, filtered sensor signals were used as inputs. One other possibility here is to use the power spectra of these signals to train the networks.

Finally, the methodology of strain prediction developed herein should be verified on other aircraft models, especially ones with different empennage configurations. The horizontal tail on a Cessna 172P is mounted to the fuselage below the vertical tail. This approach should also be verified on a mid-tail, a high T-tail, and a V-tail type empennage.

7. REFERENCES.

1. Gabriel, E.A., DeFiore, T., Locke, J.E., and Smith, H.W., “General Aviation Aircraft—Normal Acceleration Data Analysis and Collection Project, Final Report,” DOT/FAA/CT-91/20, Department of Transportation, Federal Aviation Administration, Washington, D.C., 1993.

2. Anonymous, “Fatigue Evaluation of Wing and Associated Structure on Small Airplanes,” AFS-120-73-2, Federal Aviation Administration, Washington, D.C., 1973.

3. Van Gelder, P.A., “In-Flight Tailload Measurements,” Proceedings of the 18th ICAS Congress, AIAA, Washington, D.C., 1992, pp. 1058-1066.

4. Hoffman, M.E., “A Neural Network Prototype for Predicting F-14B Strains at the B.L.10 Longeron,” NAWC Report No. NAWCADWAR-92042-60, Warminster, PA, 1992.

5. Haas, J.D., Milano, J., and Flitter, L., “Prediction of Helicopter Component Loads Using Neural Networks,” AIAA Paper 93-1301, April 1993.

6. Cook, A.B., Fuller, C.R., O'Brien, W.F., and Cabell, R.H., “Artificial Neural Networks for Predicting Nonlinear Dynamic Helicopter Loads,” AIAA Journal, Vol. 32, No. 5, May 1994, pp. 1072-1077.

7. Fausett, L., “Fundamentals of Neural Networks,” Prentice Hall, Inc., 1994.

8. DSP Development Corporation, *DaDisp Wrksheet 4.0*, 1995.

9. NeuralWare, Inc. Technical Publications Group, “A Technology Handbook for Professional II+ and NeuralWorks Explorer”, 1995, pp. 235-237.

10. NeuralWare, Inc., *NeuralWorks Professional II/Plus*, 1996.

11. Poly Software International, PSI-Plot, 1993.

12. Anonymous, MIL-HDBK-5E, Department of Defense, 1987.

APPENDIX A—AERODYNAMIC LOADING ON THE EMPENNAGE

The aerodynamic forces acting on a lifting surface such as the horizontal or vertical tail of an airplane can be represented as lift and drag at the mean aerodynamic center, together with a "pitching" couple that is independent of the angle of attack. Lift induces bending moment that results in normal and shear stresses in the spars, while drag induces bending moment that results in normal stresses in the spars and shear stresses in the panels. The couple produces torsion that results in shear stresses in the panels. This appendix provides an analytical method for estimating strains at points within the airplane flight envelope not covered by the test flight.

A.1 SIGNIFICANCE OF MEASURED STRAINS.

The strain gages in the test aircraft are located on the front spar caps, approximately one-third semispan outboard. The gages measure normal strains (stresses) induced by changes in moments about the x axis:

$$\Delta\sigma_{Y_{HT}} = \frac{\Delta M_{X_{HT}} * z}{I_{profileHT}} \quad \text{and} \quad \Delta\sigma_{Z_{VT}} = \frac{\Delta M_{X_{VT}} * y}{I_{profileVT}}$$

Consequently, the only strains measured are induced by changes in lift and drag. Only the lift is considered since drag is comparatively negligible under most flight situations.

Strains recorded for the training and testing maneuvers were performed for a subset of the aircraft flight envelope. If the entire flight envelope is considered, stresses and strains will be higher. Considering the horizontal and vertical tails as cantilever beams, maximum bending moments occur at the root of the tail surfaces. However, due to installation considerations, the strain gages are located approximately one-third of the semispan outboard. Hence, maximum strains due to bending are greater than measured strains by a proportional factor.

A.2 SPEED EFFECTS ON TAIL LOADS.

A.2.1 ROLL MANEUVER.

A.2.1.1 Change in Lift of the Horizontal Tail.

The horizontal tail is a lifting surface. Let *c(y)* be the chord of the horizontal tail at a distance *y* from the root. The lift developed by a strip element $c(y)\delta y$ is

$$L_{eq}(y)\delta y = \frac{1}{2}\rho V_{eq}{}^{2} c(y)\delta y C_L$$

In a pure roll maneuver, pitch and yaw angular motions are zero while roll rate, *p*, can be relatively "high" even for an airplane such as the C172. This roll motion results in a linear speed *py* at a distance *y* from the root of the horizontal tail. The local angle of attack is modified by an angle $\Delta\alpha$ where

$$\Delta\alpha(y) = \tan^{-1}\frac{py}{V_{eq}}$$

If *py* is small compared to V_{eq}, then

$$\Delta\alpha(y) = \frac{py}{V_{eq}}$$

The change in lift due to the change in angle of attack can be expressed as

$$\Delta L_{roll}(y)\delta y = \frac{1}{2}\rho {V_{eq}}^2 c(y)\delta y C_{L_\alpha}\Delta\alpha(y)$$

Substituting

$$\Delta L_{roll}(y)\delta y = \frac{1}{2}\rho V_{eq} c(y)\delta y C_{L_\alpha} py$$

The change in lift is linear with speed if the roll rate is constant. However, in general, roll rates may increase or decrease depending on the torsional rigidity of the wing, aileron forces, and aileron control effectiveness. In this case, for speeds V1 and V2

$$\left(\Delta L_{roll}(y)\delta y\right)_{V2} = \frac{V2}{V1}\left(\Delta L_{roll}(y)\delta y\right)_{V1}$$

The bending moment induced by the change in lift is proportional to the load; thus

$$\left(\Delta M_{roll}(y)\right)_{V2} = \frac{V2}{V1}\left(\Delta M_{roll}(y)\right)_{V1}$$

$$\Rightarrow \left(\Delta\sigma_{roll,Y}(y)\right)_{V2} = \frac{V2}{V1}\left(\Delta\sigma_{roll,Y}(y)\right)_{V1}$$

Assuming that stresses in other directions are negligible,

$$\Rightarrow \left(\Delta\varepsilon_{roll,Y}(y)\right)_{V2} = \frac{V2}{V1}\left(\Delta\varepsilon_{roll,Y}(y)\right)_{V1}$$

On the other hand, if *p* increases linearly with speed, the relationship varies as the square of the speeds.

A.2.1.2 Change in Lift (Side Force) of the Vertical Tail.

In a pure roll maneuver, the vertical tail is subjected to a side force, i.e., lift, resulting from the change in the flow angle between the relative wind and the vertical tail. The side-wash effect is comparatively negligible.

Similar to the horizontal tail, the roll rate produces a linear speed, *pz*. If *pz* is small compared to *Veq*,

$$\Delta\beta_{VT}(z) = \frac{pz}{V_{eq}}$$

The side force due to the change of angle β_{VT} can be expressed as

$$(\Delta Y_{roll}(z))_{VT}\,\delta z = \frac{1}{2}\rho {V_{eq}}^2 c_{VT}(z)\delta z(C_{L_\beta})_{VT}\,\Delta\beta_{VT}(z)$$

$$\Rightarrow (\Delta Y_{roll}(z))_{VT}\,\delta z = \frac{1}{2}\rho V_{eq} c_{VT}(z)\delta z(C_{L_\beta})_{VT}\,pz$$

If *p* is constant, the change in side force is linear with respect to speed:

$$\left(\Delta\varepsilon_{roll,Z}(y)\right)_{V2} = \frac{V2}{V1}\left(\Delta\varepsilon_{roll,Z}(y)\right)_{V1}$$

Again, if *p* increases linearly with speed, the relationship varies as the square of the speeds.

A.2.2 PUSH-PULL PITCHING MANEUVER.

During a pure push-pull maneuver, a change in loading should occur only in the horizontal tail. However, due to gyroscopic effects from spinning parts such as the engine and propeller, some vertical tail loading are induced.

A.2.2.1 Change in Lift on the Horizontal Tail.

The pitch rate is generated by an initial change in lift due to the elevator deflection. The resulting angular velocity produces a change in the tail angle of attack, and thus a subsequent change in lift

$$\Delta L(y) = \frac{1}{2}\rho {V_{eq}}^2 S(y) C_{L_\alpha}\Delta\alpha$$

This effect is known as pitch damping. For horizontal tails with zero sweep angles, $\Delta\alpha$ is constant along the span and is limited by the maximum g's permissible (3.8 g in normal category, 4.4 g in utility category) for the airplane. The pitch rate, *q*, can be shown to be

$$q = \frac{(\mathrm{n}-1)g}{V} \quad \Rightarrow \quad \Delta\alpha = \frac{q l_{HT}}{V} = \frac{(\mathrm{n}-1)g l_{HT}}{V^2}$$

Hence, the change in lift resulting from the change in angle-of-attack depends on g only and is independent of speed. Nevertheless, the initial lift that started the pitching motion that was produced by the elevator does depend on the speed:

$$\Delta L(y)_{elevator} = \frac{M_{\delta_{elevator}}}{l_{HT}} = \frac{\frac{1}{2}\rho V^2 ScCm}{l_{HT}} = \frac{\rho V^2 S(y)c(y)Cm_{\delta_{elevator}}\delta_{elevator}}{2l_{HT}}$$

Here, $Cm_{\delta_{elevator}}$ is the elevator control power and $\delta_{elevator}$ is the elevator deflection. These act to oppose each other. For a given elevator deflection, the first approximation yields,

$$\left(\Delta L(y)_{elevator}\right)_{V2} = \frac{V2^2}{V1^2}\left(\Delta L(y)_{elevator}\right)_{V1}$$

A.2.3 SIDESLIP MANEUVER.

Loads induced on the horizontal tail during sideslip maneuvers are due to the deflection of the elevator to maintain altitude. This is artificial and specific to the performance of the flight test; hence, analysis for higher speeds is not significant.

A.2.3.1 Change in Lift (Side Force) on the Vertical Tail.

The change in the side force on the vertical tail is produced by the change of sideslip angle β_{VT}

$$\Delta L(z) = \frac{1}{2}\rho V^2 S(z) C_{L_\beta}\Delta\beta_{VT}$$

$\Delta\beta_{VT}$ is essentially constant along the span of the vertical tail. Similar to the horizontal tail load during push-pull maneuver, the change in lift has a quadratic form with respect to speed

$$\Rightarrow \left(\varepsilon_{ss,Z}(z)\right)_{V2} = \frac{V2^2}{V1^2}\left(\varepsilon_{ss,Z}(z)\right)_{V1}$$

A.2.4 DUTCH-ROLL MANEUVER.

A dutch-roll maneuver is a coupling of roll and sideslip. Strains produced by dutch rolls can be calculated by superposing the strains produced by roll to those produced by sideslip.

A.2.5 STABILIZED-g TURN MANEUVER.

In a level stabilized turn, the turn rate is expressed as

$$\dot{\psi} = \frac{g\sqrt{n^2 - 1}}{V}$$

where n is determined by the angle of bank, ϕ,

$$n = \frac{1}{cos(\phi)}$$

The angular rotation about the y axis, i.e., the airplane pitch rate is

$$q = \dot{\psi} \sin\phi = \frac{g\sqrt{n^2 - 1}}{V} sin\phi$$

The pitching motion creates a change in the tail angle-of-attack, and hence its lift:

$$\Delta\alpha = \frac{q * l_{HT}}{V} = \frac{g\sqrt{n^2 - 1} * l_{HT} * sin\phi}{V^2}$$

and

$$\Delta L(y) = \frac{1}{2}\rho V^2 S(y) C_{L_\alpha} \Delta\alpha$$

The change in lift is independent of the speed and varies with g only.

A.3 VARIATION OF THE LOADS WITH ALTITUDE.

For the Cessna 172, altitudes over 10,000 ft are not common. Lift is expressed as

$$Lift = \frac{1}{2}\rho V^2 S C_L$$

where V is the true airspeed and ρ is the density of the air. In standard atmosphere, the air density decreases with altitude. At a given rpm, true airspeed corresponding to a given indicated airspeed varies with altitude. For example, at 2,500 rpm, the Pilot Operating Handbook of the C172P shows that the cruise speed decreases from 114 KIAS at 2,000 ft to 109 KIAS at 12,000 ft. Thus, if at 7,000 ft, V=112.5 KIAS

$$\left(\frac{1}{2}\rho V^2\right)_{2{,}000\,ft} \approx 1.19 \left(\frac{1}{2}\rho V^2\right)_{7{,}000\,ft}$$

This relationship shows that for the same airspeed, loads are higher at lower altitudes. However, for aircraft operating at altitudes below 10,000 ft, the effect is small.